Journal of Statistical Physics, Vol. 68, Nos. 3/4, 1992

Lattice-Gas and Lattice-Boltzmann Models of Miscible Fluids

Richard Holme[1,2] **and Daniel H. Rothman**[1]

We introduce new lattice-gas and lattice-Boltzmann models for simulating miscible fluids in two dimensions. The inclusion of a nonlocal interaction produces a lattice gas with lower diffusivity than achieved before. To overcome some observed unphysical properties of this lattice gas, we introduce a lattice-Boltzmann analogue of the model. We first formulate a miscible two-component lattice-Boltzmann model with local interactions only, and show that its diffusivity is determined by an eigenvalue of the linearized collision operator. Diffusivity is then reduced by including nonlocal interactions. The utility of the model is demonstrated by a simulation of two-dimensional viscous fingering.

KEY WORDS: Lattice gas; lattice-Boltzmann; miscible two-phase flow; viscous fingering.

1. INTRODUCTION

Lattice gases have recently been introduced as a new computational tool for the study of fluid dynamics and systems governed by related partial differential equations.[1,2] Lattice-gas models are a form of cellular automata.[3] Particles of equal mass move at constant speed on a regular lattice, under an exclusion principle which limits occupancy at each site to one particle traveling in each lattice direction. The algorithm is intrinsically discrete in space, time, and physical units. The dynamics can be divided into two parts: propagation, when particles move from one lattice node to

[1] Department of Earth, Atmospheric, and Planetary Sciences, MIT, Cambridge, Massachusetts 02139.

[2] Present address: Department of Earth and Planetary Sciences, Harvard University, Cambridge, Massachusetts 02138.

822/68/3-4-5

the next, and collision, when they interact. A collision is typically determined by conditions (the state) at that node and possibly its nearest neighbors. The realized macroscopic behavior is very close to the incompressible Navier–Stokes equations.[4–7]

While the discrete character of lattice gases is often beneficial, it leads to a high level of statistical noise. To overcome this problem, the *lattice-Boltzmann* approach has been developed, in which the particles are replaced by their mean population densities. A collision operator is defined which acts on a state vector of these probabilities. The additional assumption of no correlations between states leads to a Boltzmann equation. Models have been formulated either using a full representation of the collision operator[8] or a linearization of the operator about a local equilibrium.[9]

The choice of collisions or the form of the collision operator determines transport coefficients such as viscosity and diffusivity. Considerable effort has been made to characterize and optimize the viscosity[10–13] to attain as high a Reynolds number as possible. Diffusivity for two-phase systems has been less extensively studied. Low diffusivity is of particular interest to facilitate the study of flow dispersion. Burges and Zaleski[14] characterized diffusivity using a Chapman–Enskog expansion of the Boltzmann equation so as to maximize the Rayleigh number for convection studies. d'Humières *et al.*[15] derived optimized collision rules for minimizing the diffusivity of a lattice gas using local (single-node) concentration information. Work of Rothman and Keller[16] on a lattice-gas model for immiscible fluids actually produces a negative diffusivity.[17] In their scheme, particle directions are reorganized using nonlocal information so that, given conservation of color and momentum, they maximize particle motion toward regions of like color. This simulates interfacial forces which cause complete phase separation into homogeneous regions with stable interfaces.

Motivated by the efficiency of the phase separation mechanism, we first describe a lattice gas model similar to that in ref. 16, but without interfacial forces, and show that it has lower diffusivity than achieved before. However, statistical noise and fluctuations make the model unsuitable for applications. To overcome this, we turn to a lattice-Boltzmann analogue of the model. We first extend the linearized-Boltzmann formulation to a two-component miscible system and derive a simple relation between the diffusivity and one of the eigenvalues of the linearized collision operator. We determine the lowest diffusivity realizable with this model, and then reduce this further by including a small contribution from nonlocal interactions. We demonstrate the utility of the new method by presenting some results of a simulation of two-dimensional miscible viscous fingering.

2. A NONLOCAL LOW-DIFFUSIVITY LATTICE GAS

We first develop a low-diffusivity miscible lattice-gas model by including nonlocal interactions, using a variant of an FHP-II lattice gas.[5] This model is constructed on a triangular lattice, and has seven allowed states per site, one particle with each of the six possible velocities and one rest particle. A two-phase system is defined by giving each particle an additional property, described as red or blue "color."

We use the following notation. The ith velocity vector is denoted by $\mathbf{c}_i$; $\mathbf{c}_0 = \mathbf{0}$ and $\mathbf{c}_1$ through $\mathbf{c}_6$ are unit vectors connecting neighboring sites on the triangular lattice. The directions are defined in Fig. 1. The Boolean variables $r_i(\mathbf{x}) \in \{0, 1\}$ and $b_i(\mathbf{x}) \in \{0, 1\}$ indicate the presence or absence of a red or blue particle with velocity $\mathbf{c}_i$ at lattice site $\boldsymbol{x}$. The configuration at a site is completely described by the two 7-bit variables $r = \{r_i, i = 0,..., 6\}$ and $b = \{b_i, i = 0,..., 6\}$. There may be only one particle in any given state, and this particle may be either red or blue.

The outcome of a collision $(r \to r'', b \to b'')$ is determined as a two-stage process via an intermediate state (r', b'). First, the particle velocities are rearranged without reference to color. A new configuration is selected at random from those satisfying the constraints of colored mass conservation,

$$\sum_i r_i' = \sum_i r_i, \qquad \sum_i b_i' = \sum_i b_i \tag{1}$$

and color-blind momentum conservation

$$\sum_i \mathbf{c}_i (r_i' + b_i') = \sum_i \mathbf{c}_i (r_i + b_i) \tag{2}$$

Second, given this new mass distribution, the color is rearranged so as to align the colored velocities with the local color gradient. We define the

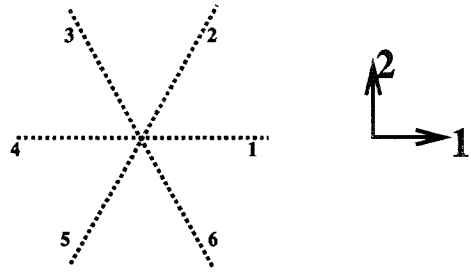

Fig. 1. Definition of lattice directions.

local color flux to be the difference between the net red momentum and net blue momentum at site $\mathbf{x}$:

$$\mathbf{q}[r(\mathbf{x}), b(\mathbf{x})] \equiv \sum_i \mathbf{c}_i [r_i(\mathbf{x}) - b_i(\mathbf{x})] \tag{3}$$

The local color field $\mathbf{f}(\mathbf{x})$ is defined to be the vectorial sum of the differences between the number of reds and the number of blues at neighboring sites [i.e., the microscopic gradient of the signed (red minus blue) color density]:

$$\mathbf{f}(\mathbf{x}) \equiv \sum_i \mathbf{c}_i \sum_j [r_j(\mathbf{x} + \mathbf{c}_i) - b_j(\mathbf{x} + \mathbf{c}_i)] \tag{4}$$

We then choose r'' and b'' such that $\mathbf{f} \cdot \mathbf{q}(r'', b'')$, the projection of the color flux in the direction of the color field, is maximized, subject to the condition $r_i'' + b_i'' = r_i' + b_i'$ (the occupancy of a state is unchanged). Note that if there is more than one outcome in either stage of the collision process that satisfies the requirements equally well, the result is decided by random selection from those outcomes.

This algorithm is closely related to the immiscible lattice gas (ILG) model of Rothman and Keller,[16] with one important difference. In the earlier model, $\mathbf{f} \cdot \mathbf{q}$ is maximized by rearranging color and momentum simultaneously. In the new model, particle velocities are rearranged without reference to color, after which color is rearranged given the new mass configuration. Breaking the collision into two stages removes the influence of the color field on collision dynamics, and so eliminates the surface tension.

Figure 2 presents a comparison of the diffusivity of the new model with two models studied by d'Humières *et al.*[15] The "limited diffusion" model minimizes diffusion using local color information, while the "self-diffusion" model does not optimize diffusivity. We follow McNamara[18] in characterizing the diffusivity by establishing a steady-state color gradient and measuring the resulting flux. We use a lattice of 64×128 lattice units with wraparound boundary conditions. The color gradient is maintained in the long direction by recoloring all particles red at one end of the lattice and blue at the other. Considerable averaging is necessary to damp statistical fluctuations. The data for the established algorithms show good agreement with previous work.[15] Unsurprisingly, the self-diffusion model has the highest diffusivity. At moderate and high densities our new model has lower diffusivity than the limited diffusion algorithm.

However, statistical fluctuations make the new model inappropriate for hydrodynamic applications. Figure 3 shows the mixing of two initially

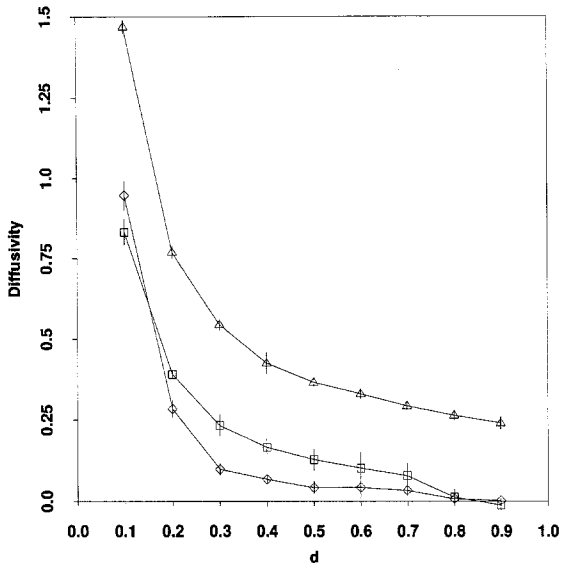

Fig. 2. Comparison of diffusion coefficients for different lattice-gas models. (◇) New algorithm. (□) Limited diffusion. (△) Self-diffusion.

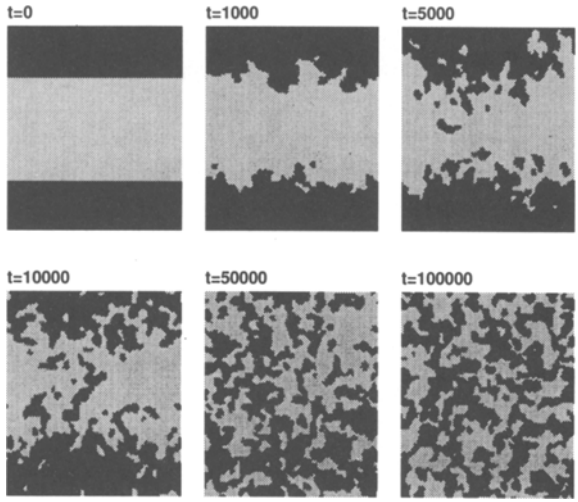

Fig. 3. Nonequilibrium behavior of lattice-gas model. Time is given in time steps.

separated phases. Random fluctuations cause "fingering" of the interface between the phases. If these fingers become sufficiently thin, they detach, and the system evolves to a mixture of bubbles of fluid, constantly decomposing, changing morphology, and reconnecting. An initially uniform color distribution approaches this same equilibrium.

Though this lattice gas is unsuitable for applications, we later apply these ideas to the construction of a low-diffusivity lattice-Boltzmann model.

3. A LATTICE-BOLTZMANN MODEL FOR TWO MISCIBLE FLUIDS

3.1. Mathematical Formulation

We may mathematically describe a lattice-gas collision by the equation

$$\mathbf{Y}'(\mathbf{x}, t) = \Omega(\mathbf{Y}(\mathbf{x}, t)) \tag{5}$$

where $\mathbf{Y}$ is a state vector at position $\mathbf{x}$, Ω is a collision operator, and the primed notation describes the postcollision configuration. The elements of $\mathbf{Y}$ are Boolean variables, taking values 1 or 0 to describe the presence or absence of a particle in a particular state. We may replace this by a vector of probabilities describing the likelihood of a particle being found in each state. If we further assume the Boltzmann approximation that the probabilities are uncorrelated, the collision equation is considerably simplified. Previous workers[4,5,14,17–19] have derived theoretical results for lattice-gas behavior using this approximation, and have shown it to be valid.

We consider a model without rest particles. We define the state at a site by six 2-vectors composed of the mean particle populations for each color, which we write $\mathbf{N}_i = (R_i, B_i)$. We divide this into equilibrium and nonequilibrium components, writing $\mathbf{N}_i = \mathbf{N}_i^{\text{eq}} + \mathbf{N}_i^{\text{neq}}$, where the equilibrium distribution is that part of the state vector which is invariant under action of the collision operator. Loss of Galilean invariance is a well-known problem in lattice gases.[5,14] By making a suitable choice of the equilibrium we may avoid this.[20] The equilibrium is thus given by

$$\begin{aligned} R_i^{\text{eq}} &= d_r(1 + 2c_{i\alpha}v_\alpha + 4Q_{i\alpha\beta}v_\alpha v_\beta) \\ B_i^{\text{eq}} &= d_b(1 + 2c_{i\alpha}v_\alpha + 4Q_{i\alpha\beta}v_\alpha v_\beta) \end{aligned} \tag{6}$$

where $d_r = \frac{1}{6}\sum R_i$, $d_b = \frac{1}{6}\sum B_i$, v_α is the fluid velocity in one of the two orthogonal directions shown in Fig. 1, $c_{i\alpha}$ is the α component of the characteristic lattice velocity in lattice direction i, and

$$Q_{i\alpha\beta} = c_{i\alpha}c_{i\beta} - \tfrac{1}{2}\delta_{\alpha\beta} \tag{7}$$

In addition, it is convenient at this stage to define a state density $d = d_r + d_b$, which takes values from 0 to 1.

We linearize the collision equation about the given equilibrium. This leads to[9]

$$\mathbf{N}_i'(\mathbf{x}, t) = \mathbf{N}_i(\mathbf{x}, t) + \sum_{j=1}^{6} \boldsymbol{\omega}_{ij} \mathbf{N}_j^{\text{neq}}(\mathbf{x}, t) \tag{8}$$

Each $\boldsymbol{\omega}_{ij}$ is a 2×2 matrix. To simplify the mathematics, we change our representation from six 2-vectors to the 12-vector

$$\mathbf{Y} = (R_1, B_1, R_2, B_2, ..., R_6, B_6)^T \tag{9}$$

with the nonequilibrium component written as

$$\mathbf{y} = (r_1, b_1, r_2, b_2, ..., r_6, b_6)^T \tag{10}$$

Substituting in Eq. (8),

$$y_i' - y_i = \sum_{j=1}^{12} \Omega_{ij} y_j \tag{11}$$

where we have implicitly defined the collision operator Ω_{ij}.

The collision operator Ω_{ij} has 16 independent elements which define the model's behavior. This is described in some detail in Appendix A. There we show that, given conservation of momentum, there will always exist a pair of right-eigenvectors of the operator whose associated eigenvalue λ_D defines the diffusivity by the relation

$$D = -\frac{1}{2}\left(\frac{1}{\lambda_D} + \frac{1}{2}\right) \tag{12}$$

The model also has two characteristic kinematic viscosities which are related to other eigenvalues λ_ν by

$$\nu = -\frac{1}{4}\left(\frac{1}{\lambda_\nu} + \frac{1}{2}\right) \tag{13}$$

which is an expression given previously by a number of authors.[10,13,19,21] All eigenvalues of Ω_{ij} are required to be between 0 and -2, or else nonequilibrium fluctuations grow and the linearization of the operator is invalid. In principle, but not necessarily in practice, we can assign any positive value to either transport coefficient.

3.2. Numerical Experiments

The diffusion coefficient is determined as for the lattice gas model. Due to the lower fluctuations of the lattice-Boltzmann model compared with the lattice gas, we may use much smaller lattices of dimension 64×4 lattice units. We used a state density $d = 0.5$. Figure 4 demonstrates that the derived eigenvalue relation holds over many orders of magnitude. It should be noted, however, that the color flux saturates at a maximum value of $4d$. Thus, for a given required color gradient $|\nabla\sigma|$ there is a maximum usable diffusivity $D_{\max} = 4d/|\nabla\sigma|$.

The low-diffusivity end of the range is potentially more useful. Figure 5 shows that the theory is valid up to an eigenvalue of about -1.95, which corresponds to a diffusivity of 7.27×10^{-3} lattice units squared per time step. We suggest that this represents a lower limit for the diffusivity achievable by this model, below which discrete lattice effects become significant. To achieve yet lower diffusivity, we introduce another approach, described below.

Kinematic viscosity has also been characterized by studying the decay of a standing wave, as in ref. 22. Stable behavior obeying the eigenvalue relation was seen for viscosities between 1.5 and 5×10^{-4} lattice units squared per time step.

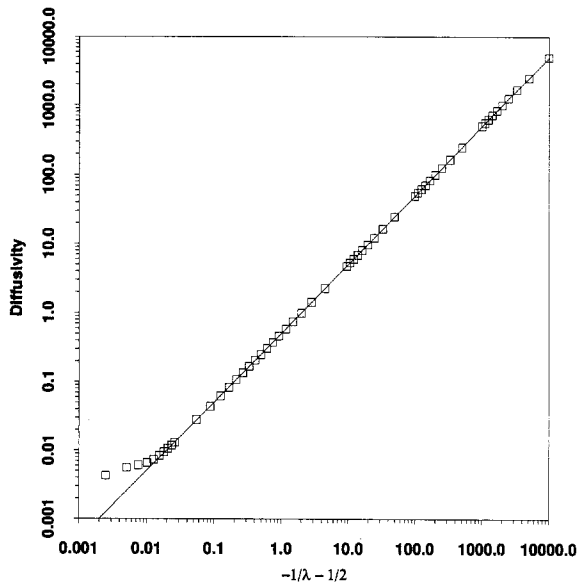

Fig. 4. Numerical confirmation of diffusivity eigenvalue relation. The solid line is calculated from the theoretical relation. Error bars are many times smaller than the symbols used to mark the data points.

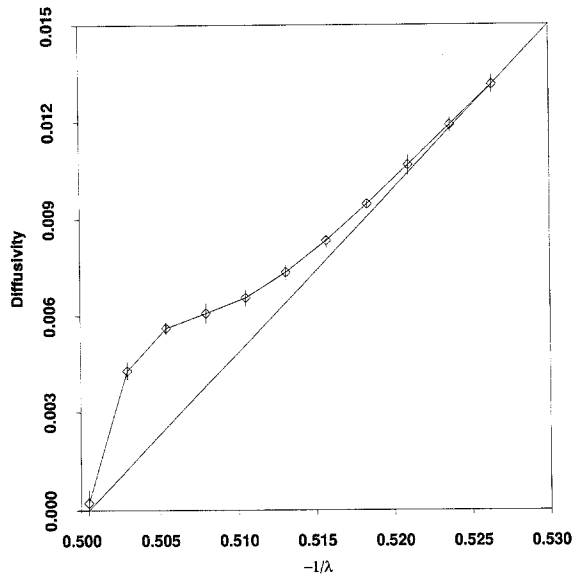

Fig. 5. Divergence from linear relationship at low diffusivities. The straight line is the theoretical relationship.

We note that such static and well-defined measurements of transport coefficients do not necessarily carry over to dynamic simulations. The finite time step and lattice unit impose a lower limit on the diffusivity that can be accurately simulated in a given flow situation. This limit is consistent with stability criteria for finite-difference solutions of a one-dimensional convection-diffusion equation.[23]

4. A LOWER DIFFUSIVITY LATTICE-BOLTZMANN MODEL

The lattice-Boltzmann model introduced above achieves optimization of diffusivity using information from only one site, and so can be regarded as the lattice-Boltzmann counterpart of the limited-diffusion lattice-gas model of d'Humières *et al.* We now introduce a lattice-Boltzmann formulation based upon the nonlocal lattice gas rule developed in Section 2. At each collision, a local two-color linearized operator is applied. We then rearrange a small fraction $\alpha\,|\nabla\sigma|/d$ of the color by the nonlocal algorithm, where α is a free parameter, $|\nabla\sigma|$ is the magnitude of the color gradient, and d is the state density. This parametrization preserves Fickian behavior

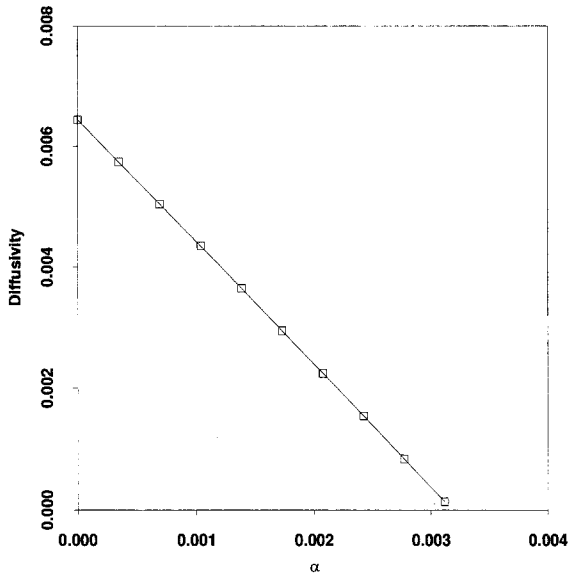

Fig. 6. Diffusivity for small addition of nonlocal algorithm.

and keeps diffusivity independent of density. For low diffusivities, it is shown in Appendix B that

$$D = D_0 - 2\alpha \tag{14}$$

where D_0 is the diffusivity for local interactions only. Care must be taken that too much weight is not given to the nonlocal algorithm, which would result in $D < 0$.

An experimental verification of Eq. (14) is presented as Fig. 6. We set the diffusivity eigenvalue to $\lambda_D = -1.95$, which is sufficiently low for Eq. (14) to apply. Measurements were made using a lattice of size 64×8 lattice units at state density 0.5. Other results indicate that the diffusivity is independent of density, as expected.

We note that if α is set so as to rearrange all the color at each site, this model is equivalent to the lattice-Boltzmann model for immiscible fluids of Gunstensen *et al.*[21] for the case in which surface tension vanishes.

5. A SIMULATION OF HELE-SHAW FLOW

We demonstrate qualitatively the utility of our new model with a simulation of miscible two-phase flow in a Hele-Shaw cell. The problem is of particular relevance as it is an exact dynamical analogue of two-dimen-

sional, two-phase flow in porous media.[24,25] The Hele-Shaw cell consists of fluid confined between two parallel and closely spaced plates. The most interesting behavior is produced when a more viscous fluid is displaced from between the plates by injection of a less viscous fluid. With immiscible fluids the development of the system is governed by the surface tension between the fluids, leading to viscous fingering of the interface known as the Saffman–Taylor instability.[24] With no surface tension present, other behavior is possible. Homsy[25] reviews what is known about the behavior of miscible flows.

The solution for an equilibrium single-phase flow in a Hele-Shaw cell is well known.[24] Application of no-slip boundary conditions at vertically-oriented plates gives a parabolic velocity profile, with mean velocity

$$\mathbf{v} = -\frac{b^2}{12\nu}\left(\frac{\nabla P}{\rho} - \mathbf{g}\right) \tag{15}$$

Here b is the plate separation, ν is the dynamic viscosity, ρ is the density, ∇P is the applied pressure gradient, and $\mathbf{g}$ is the acceleration due to gravity. This solution also holds for regions of uniform composition. In mixed regions, the development of the system depends on the variation of viscosity with composition, and hence the development of the concentration field. The problem is then to track regions of varying composition. This is straightforward using our lattice-Boltzmann model.

A linear stability analysis of the interface between the two fluids was given by Chouke *et al.*[26] Homsy[25] gives a summary of this for the miscible case. The interface is shown to be increasingly unstable at shorter wavelengths, with a cutoff at very short wavelengths due to dispersion. More recently, Bensimon *et al.*[27] and others have used a conformal mapping technique to describe the evolution of the interface between two fluids in the limit of infinite Peclet number (no mixing). They find that the interface will develop one or more cusps in finite time, pointing into the more viscous fluid, and typically of power $\frac{2}{3}$,[28] after which the equations no longer have a solution. These cusps occur for a wide range of initial conditions.[29] The cusps are classified by defining a local Cartesian coordinate system with origin at the cusp point and y axis parallel to the cusp. In these coordinates the interface has the local functional form $y^3 = O(x^2)$.[30]

To simulate flow in a Hele-Shaw call, we extend our model to include effects of gravity, pressure, and frictional drag due to the plates. Gravity is applied by rearranging a small fraction of the mean particle populations at each site so as to drive the "light" fluid upward and the "heavy" fluid downward.[14,31] The viscous drag is achieved similarly, by rearranging a

small fraction of the mean particle populations isotropically between the states at each site so as to reduce the net momentum. A balance between gravity and the required velocity in Eq. (15) enables us to parametrize the viscous force in terms of plate separation. A pressure gradient can be established by the addition of momentum to one edge of the simulation. For the purpose of calculating the viscous drag, we define the viscosity of a mixed region to be a weighted average of the viscosities of the separate phases.

By varying the forcing parameters, a wide variety of behavior is observed. We include as Fig. 7 contour plots of concentration from a representative simulation. Here we apply no pressure gradient, so that the region of interest (where the fluids mix) remains in the center of the simulation. We use a lattice-Boltzmann model with local interactions only, with the diffusivity eigenvalue set to $\lambda_D = -1.95$. The lighter fluid is a factor of two less viscous than the heavier fluid, and initially occupies the bottom half of the lattice. The lattice size is 128×128 lattice units, and the effective plate separation is 5 lattice units. Using the lattice width L for a length scale, and a velocity scale U calculated from the gravitational forcing by means of Eq. (15), we can define a Peclet number of $Pe = UL/D \approx 1700$. We define a dimensionless diffusive time scale $T = tU^2/D = 1.5t$. The two fluids are initially stationary, and the interface between them is horizontal. It was

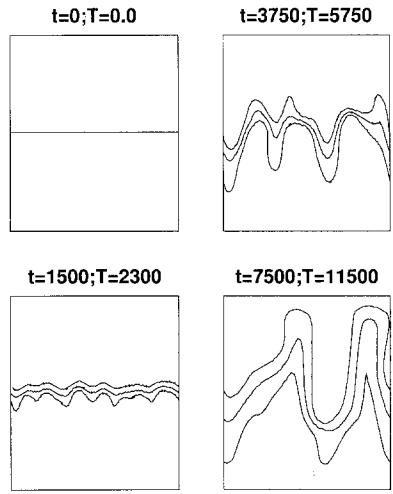

Fig. 7. Contour plots for Hele-Shaw flow simulation. Contours are for 1/4, 1/2, and 3/4 light fluid. The lighter, less viscous fluid is on the bottom. The lattice is 128×128; time is given in time steps t, and in terms of the diffusive time scale T.

found that any initially imposed perturbation in the interface was damped by diffusion before the instability developed. We place walls at the top and bottom of the lattice to contain the cell, and apply periodic boundary conditions laterally. Bensimon *et al.*[27] have used these periodic conditions in theoretical calculations. They also refer to work of Aribert,[32] who studied the effect of periodic boundary conditions experimentally using a cylindrical Hele-Shaw cell.

As can be seen from Fig. 7, the initially horizontal interface becomes unstable at small length scales, initiated by floating-point errors. Application of the results from linear stability theory gives a wavelength cutoff for the instability of less than one lattice unit, so we would expect the initial instability to be at the lattice-unit scale. The scale of the instability increases until its dominant wavelength is of the same order as the simulation width. The instability grows, and the concentration contours develop sharp points, consistent with the 2/3 power cusps expected from theory, which then smooth into fingers. An example of such a cusp can be seen at the right-hand side of the last contour plot of Fig. 7. Smoothing occurs when the scale of the cusp is less than one lattice unit. Bensimon *et al.* note that in a real system, any surface tension, however small, will prevent the formation of cusps once the curvature is sufficiently great. Further work is necessary to determine whether or not the results after the appearance of the cusp have any validity in terms of a small surface tension parameter.

Tan and Homsy[33] have studied the similar problem of miscible viscous fingering driven by pressure gradients. They use a spectral method for their simulations, which exhibit features in common with ours, in particular the cascade from small to large length scales of the instability, but they do not observe development of discontinuities in the interface. However, they describe tip-splitting of the fingers at certain Peclet numbers and viscosity ratios, which we do not observe. This difference may be due to the different forcing mechanism, or to a different parametrization of the viscosity of the mixed fluids.

6. CONCLUSIONS

We have introduced three new lattice-gas techniques for studying low-diffusivity miscible fluids. A lattice gas using nonlocal interactions achieved low diffusivities, but at the cost of locally non-Fickian behavior. A lattice-Boltzmann approach allows simulation of a wide range of diffusivities. The minimum diffusivity achievable may be further reduced by the application of nonlocal collisions.

We use two dimensionless numbers to describe the range of our model.

The Schmidt number, which measures the ratio of diffusion of momentum to diffusion of color, is defined by

$$Sc = \frac{\nu}{D} \tag{16}$$

The concentration Peclet number, which measures the ratio of advection to diffusion, is defined by

$$Pe = \frac{LU}{D} \tag{17}$$

where L and U are suitable length and velocity scales for the flow under study. As noted earlier, the maximum diffusivity $D_{\max}$ is determined by the precise nature of the simulation. Setting $D_{\max} = 10$, an arbitrary but reasonable value, allows a range of Schmidt numbers $5 \times 10^{-5} < Sc < 3 \times 10^{3}$. This range is greater than for lattice gases because in the lattice-Boltzmann formulation viscosity and diffusivity are completely decoupled. Bounds on the Peclet number depend on the length and velocity scales L and U of the motion, but we may write $0.67LU < Pe < 2000LU$.

The utility of the technique has been successfully demonstrated by the simulation of viscous fingering in a Hele-Shaw cell. Further applications, in particular to two-phase miscible flow in microscopic models of porous media, seem promising.

APPENDIX A. DEFINITION OF THE LINEARIZED-BOLTZMANN OPERATOR

In this Appendix we show how the transport coefficients of the miscible two-phase lattice-Boltzmann model are defined by the eigenvalues and eigenvectors of the collision operator. We present results for two dimensions. Generalization to three dimensions is straightforward.

To achieve isotropic macroscopic behavior in two dimensions, the collision operator must have sixfold rotational and mirror symmetries.[13] For $1 \leqslant i, j \leqslant 6$, we may write $\omega_{ij} = \omega_{|i-j|}$, where ω_{ij} is as defined for Eq. (8). We therefore denote the matrices by ω^0, ω^{60}, etc., where the superscript is the angle in degrees between the directions i and j. Using the compact notation defined by Eq. (11), we now write the collision operator

$$\Omega = \begin{pmatrix} \omega^0 & \omega^{60} & \omega^{120} & \omega^{180} & \omega^{120} & \omega^{60} \\ \omega^{60} & \omega^0 & \omega^{60} & \omega^{120} & \omega^{180} & \omega^{120} \\ \omega^{120} & \omega^{60} & \omega^0 & \omega^{60} & \omega^{120} & \omega^{180} \\ \omega^{180} & \omega^{120} & \omega^{60} & \omega^0 & \omega^{60} & \omega^{120} \\ \omega^{120} & \omega^{180} & \omega^{120} & \omega^{60} & \omega^0 & \omega^{60} \\ \omega^{60} & \omega^{120} & \omega^{180} & \omega^{120} & \omega^{60} & \omega^0 \end{pmatrix} \tag{A1}$$

This can be seen to be block circulant. From an extension of the theory of circulant matrices (e.g., ref. 34), it can be demonstrated that the right-eigenvectors of this matrix are in pairs of the form

$$\mathbf{v}_\mu = (\alpha, \beta, \alpha\xi_\mu, \beta\xi_\mu, \alpha\xi_\mu^2, \beta\xi_\mu^2, \alpha\xi_\mu^3, \beta\xi_\mu^3, \alpha\xi_\mu^4, \beta\xi_\mu^4, \alpha\xi_\mu^5, \beta\xi_\mu^5)^T \quad \text{(A2)}$$

with corresponding left-eigenvectors

$$\mathbf{u}_\mu = (\gamma, \delta, \gamma\xi_\mu^{-1}, \delta\xi_\mu^{-1}, \gamma\xi_\mu^{-2}, \delta\xi_\mu^{-2}, \gamma\xi_\mu^{-3}, \delta\xi_\mu^{-3}, \gamma\xi_\mu^{-4}, \delta\xi_\mu^{-4}, \gamma\xi_\mu^{-5}, \delta\xi_\mu^{-5}) \quad \text{(A3)}$$

Here μ is an integer between 0 and 5, $\xi_\mu = \exp(2\pi i\mu/6)$, and (α, β) and $(\gamma, \delta)^T$ are respectively the right- and left-eigenvectors of the matrices

$$\mathbf{M}_\mu = \boldsymbol{\omega}^0 + 2\cos\left(\frac{\mu\pi}{3}\right)\boldsymbol{\omega}^{60} + 2\cos\left(\frac{2\mu\pi}{3}\right)\boldsymbol{\omega}^{120} + \cos(\mu\pi)\,\boldsymbol{\omega}^{180} \quad \text{(A4)}$$

Due to the required mirror symmetry, only four of these matrices $\mathbf{M}_\mu$ are distinct, giving rise to a total of eight distinct eigenvalues and eight eigenvector pairs to describe the system. These are defined by the 16 independent elements of the collision matrix. Provided these are chosen such that the operator is not defective, the eigensystem provides a complete basis for the lattice dynamics.

We require that the collision satisfy conservation of mass for each color and total momentum. The total change in red mass at a site is thus given by

$$\sum_{i=1}^{6} (r_i' - r_i) = 0 \quad \text{(A5)}$$

with a similar expression for blue mass. These conditions require that the vectors

$$(1, 0, 1, 0, \ldots, 1, 0); \qquad (0, 1, 0, 1, \ldots, 0, 1) \quad \text{(A6)}$$

are left-eigenvectors of the collision matrix with eigenvalue 0. These are the vector pair $\mathbf{u}_0$. For conservation of momentum, we require that

$$\begin{aligned} &(c_{11}, c_{11}, \ldots, c_{61}, c_{61}) \\ &(c_{12}, c_{12}, \ldots, c_{62}, c_{62}) \end{aligned} \quad \text{(A7)}$$

be left-eigenvectors with eigenvalue 0. By referring to Fig. 1, we can write these explicitly as

$$\begin{aligned} &(1, 1, \cos(\pi/3), \cos(\pi/3), \cos(2\pi/3), \cos(2\pi/3), \ldots, \cos(5\pi/3), \cos(5\pi/3)) \\ &(0, 0, \sin(\pi/3), \sin(\pi/3), \sin(2\pi/3), \sin(2\pi/3), \ldots, \sin(5\pi/3), \sin(5\pi/3)) \end{aligned} \quad \text{(A8)}$$

where the angle is measured positive from the 1-direction. From Eq. (A3) we see that these are both linear combinations of $\mathbf{u}_1$ and $\mathbf{u}_5$, and thus valid left-eigenvectors of the collision operator. There are therefore six equations of constraint on the elements of the collision operator, two due to each independent conservation relation.

We now determine the characteristic diffusivity of the operator. In analogy to the calculation by Hénon[10] of the kinematic viscosity of a lattice gas, we consider a linear color gradient of magnitude $2G$ in the 2-direction (defined in Fig. 1), which produces a uniform flux of color, but at constant mass state density d. Using the equilibrium equations (6), we get

$$\begin{aligned} R_i &= d_{r0} + \frac{G}{6} x_2 + r_i \\ B_i &= d_{b0} - \frac{G}{6} x_2 + b_i \end{aligned} \tag{A9}$$

where d_{r0} and d_{b0} are values of the state density for each color at $x_2 = 0$, and r_i and b_i are the local anisotropies which maintain the color gradient. We define microscopic momentum fields for each color by

$$F_\alpha^r = \sum_i R_i c_{i\alpha}, \qquad F_\alpha^b = \sum_i B_i c_{i\alpha} \tag{A10}$$

where α represents one of the two orthogonal directions 1 and 2 defined in Fig. 1. By assumption,

$$\begin{aligned} F_1^r &= F_1^b = 0 \\ F_2^r &= -F_2^b = F \end{aligned} \tag{A11}$$

where F is a constant (dependent on G) to be determined. We assume that the anisotropy in the color distribution, like the color flux, is independent of position. This gives

$$\begin{aligned} \sum_{i=1}^{6} r_i &= 0, & \sum_{i=1}^{6} b_i &= 0 \\ \sum_{i=1}^{6} r_i c_{i1} &= 0, & \sum_{i=1}^{6} b_i c_{i1} &= 0 \\ \sum_{i=1}^{6} r_i c_{i2} &= F, & \sum_{i=1}^{6} b_i c_{i2} &= -F \end{aligned} \tag{A12}$$

The propagation equation from one time step to the next can be written

$$R_i(\mathbf{x}+\mathbf{c}_i, t+1) = R_i'(\mathbf{x}, t) \tag{A13}$$

with a similar equation for B_i. By assuming a steady state over time, this reduces to

$$R_i(\mathbf{x}+\mathbf{c}_i) = R_i'(\mathbf{x}) \tag{A14}$$

Using (A9), we obtain

$$r_i(\mathbf{x}) - r_i'(\mathbf{x}) = -G/6c_{i2} \tag{A15}$$

with a similar equation for b_i. Combining with the collision Eq. (11), we write these equations in matrix form:

$$\mathbf{\Omega y} = \frac{G}{6}\mathbf{z} \tag{A16}$$

where $\mathbf{y}$ is the state vector and $\mathbf{z} = (c_{12}, -c_{12}, \ldots, c_{62}, -c_{62})^T$.

The vector $\mathbf{z}$ can be constructed from right-eigenvectors $\mathbf{v}_1$ and $\mathbf{v}_5$ and is orthogonal to the left-eigenvectors required for momentum conservation given in Eqs. (A7). Hence, by biorthogonality $\mathbf{z}$ is always a required right-eigenvector of the operator. $\mathbf{y}$ is a scalar multiple of $\mathbf{z}$, and from Eqs. (A12) we derive the scale factor to be $F/3$. The steady-state color distribution is given by

$$\begin{aligned} R_i &= d_{r0} + \frac{G}{6}x_2 + \frac{F}{3}c_{i2} \\ B_i &= d_{b0} - \frac{G}{6}x_2 - \frac{F}{3}c_{i2} \end{aligned} \tag{A17}$$

F and G are related by

$$\frac{F}{G} = \frac{1}{2\lambda_D} \tag{A18}$$

where λ_D is the eigenvalue of Ω corresponding to the eigenvector $\mathbf{z}$.

For a simple concentration gradient, we expect the flow of color to obey Fick's law,

$$J = -D\frac{d\sigma}{dx_2} \tag{A19}$$

where J is the color flux across a line per unit length, D is the diffusion coefficient, and σ is the color density, defined per unit area. Due to the triangular lattice,

$$\frac{d\sigma}{dx_2} = \frac{4}{\sqrt{3}}G \tag{A20}$$

Following McNamara[18] and others, we calculate the flux crossing a line between two rows of lattice points. This is

$$J = R_2(\mathbf{x}+\mathbf{c}_2) - B_2(\mathbf{x}+\mathbf{c}_2) + R_3(\mathbf{x}+\mathbf{c}_3) - B_3(\mathbf{x}+\mathbf{c}_3) - R_5(\mathbf{x}) + B_5(\mathbf{x}) - R_6(\mathbf{x}) + B_6(\mathbf{x}) \tag{A21}$$

Using Eqs. (A17) and (A19)–(A21), we find that the diffusivity is

$$D = -\frac{F}{G} - \frac{1}{4} \tag{A22}$$

Using Eq. (A18), we can write this in terms of the relevant eigenvalue of the collision operator:

$$D = -\frac{1}{2}\left(\frac{1}{\lambda_D} + \frac{1}{2}\right) \tag{A23}$$

We now briefly discuss the other degrees of freedom of the operator. The eigenvalues corresponding to the eigenvectors $\mathbf{v}_2$ and $\mathbf{v}_4$ define the model's kinematic viscosity. This can be shown from a Chapman–Enskog expansion of the particle distribution function[19] or by the more physical arguments of Hénon.[10] The viscosity is well defined for mixtures of the two species whose relative proportions are given by the eigenvectors. The eigenvalue relations are the same as the one-color expression which has been given by a number of authors,[10,13,19,21]

$$\nu = -\frac{1}{4}\left(\frac{1}{\lambda_\nu} + \frac{1}{2}\right) \tag{A24}$$

The eigenvectors $\mathbf{v}_3$ have no direct relation to any transport properties.[35] To make the algorithm as stable as possible, the corresponding eigenvalues are set to -1, so that perturbations in this eigendirection die away immediately.

APPENDIX B. ANALYSIS OF NONLOCAL COLLISION ALGORITHM

In this Appendix, we extend the analysis in Appendix A to the nonlocal algorithm.

To simplify the mathematical development, we will assume that the red and blue fluids are present in equal proportions. Consider the

steady-state color distribution given by Eqs. (A17). Application of the local linearized collision operator to this produces

$$\begin{aligned} R_i'(x_2) &= d_{r0} + \frac{G}{6} x_2 + (1+\lambda_D)\frac{F}{3} c_{i2} \\ B_i'(x_2) &= d_{b0} - \frac{G}{6} x_2 - (1+\lambda_D)\frac{F}{3} c_{i2} \end{aligned} \tag{B1}$$

We then apply the nonlocal algorithm with the scaling $\alpha\,|\nabla\sigma|/d$. This takes total mass $\alpha\,|\nabla\sigma|$ and redistributes its color to oppose the local color gradient. By our definitions, $|\nabla\sigma| = 4G/\sqrt{3}$. The resulting color distribution can then be written

$$\begin{aligned} R_i''(x_2) &= \left(1 - \frac{4G\alpha}{\sqrt{3}\,d}\right)\left(d_{r0} + \frac{G}{6} x_2 + (1+\lambda_D)\frac{F}{3} c_{i2}\right) \\ &\quad + \frac{2G\alpha}{\sqrt{3}} + \frac{4G\alpha}{3} c_{i2} \\ B_i''(x_2) &= \left(1 - \frac{4G\alpha}{\sqrt{3}\,d}\right)\left(d_{r0} - \frac{G}{6} x_2 - (1+\lambda_D)\frac{F}{3} c_{i2}\right) \\ &\quad + \frac{2G\alpha}{\sqrt{3}} - \frac{4G\alpha}{3} c_{i2} \end{aligned} \tag{B2}$$

Using the steady-state propagation equation (A14), we require this to be equal to

$$\begin{aligned} R_i(x_2 + c_{i2}) &= d_{r0} + \frac{G}{6}(x_2 + c_{i2}) + \frac{F}{3} c_{i2} \\ B_i(x_2 + c_{i2}) &= d_{b0} - \frac{G}{6}(x_2 + c_{i2}) - \frac{F}{3} c_{i2} \end{aligned} \tag{B3}$$

Assuming α to be small, we obtain the equation

$$\frac{G}{2} = F\lambda_D + 4G\alpha \tag{B4}$$

Using (A22), we may write this in terms of the diffusivity

$$D = \frac{8\alpha - 1}{2\lambda_D} - \frac{1}{4} \tag{B5}$$

Writing λ_D in terms of D_0, the diffusivity for the local algorithm only, we obtain

$$D = D_0 - 8\alpha\left(D_0 + \frac{1}{4}\right) \tag{B6}$$

For small values of D_0, this simplifies to the expression given earlier as Eq. (14),

$$D = D_0 - 2\alpha \tag{B7}$$

This theory is approximate for nonequal color concentrations. However, simulations suggest that it remains a good approximation over a wide range of conditions.

ACKNOWLEDGMENTS

This work was supported by NSF Grant 9017062-EAR, and by the sponsors of the MIT Porous Flow Project. R.H. was supported through tenure as a Kennedy Scholar. R.H. thanks Andrew Gunstensen for invaluable technical assistance.

REFERENCES

1. U. Frisch, B. Hasslacher, and Y. Pomeau, *Phys. Rev. Lett.* **56**:1505 (1986).
2. G. D. Doolen, ed., *Lattice Gas Methods for Partial Differential Equations* (Addison-Wesley, 1990).
3. S. Wolfram, ed., *Theory and Applications of Cellular Automata* (World Scientific, Singapore, 1986).
4. S. Wolfram, *J. Stat. Phys.* **45**:471 (1986).
5. U. Frisch, D. d'Humières, B. Hasslacher, P. Lallemand, Y. Pomeau, and J.-P. Rivet, *Complex Systems* **1**:648 (1987).
6. L. Kadanoff, G. McNamara, and G. Zanetti, *Phys. Rev. A* **40**:4527 (1989).
7. G. Zanetti, *Phys. Rev. A* **40**:1539 (1989).
8. G. McNamara and G. Zanetti, *Phys. Rev. Lett.* **61**:2332 (1988).
9. F. Higuera and J. Jimenez, *Europhys. Lett.* **9**:663 (1989).
10. M. Hénon, *Complex Systems* **1**:763–789 (1987).
11. B. Dubrulle, U. Frisch, M. Hénon, and J.-P. Rivet, *J. Stat. Phys.* **59**:1187–1226 (1990).
12. D. H. Rothman, *J. Stat. Phys.* **56**:1119 (1989).
13. F. Higuera, S. Succi, and R. Benzi, *Europhys. Lett.* **9**:345 (1989).
14. C. Burges and S. Zaleski, *Complex Systems* **1**:31 (1987).
15. D. d'Humières, P. Lallemand, J. P. Boon, D. Dab, and A. Noullez, Fluid dynamics with lattice gases, in *Chaos and Complexity*, R. Livi, S. Ruffo, S. Cilberto, and M. Buiatti, eds. (World Scientific, Singapore, 1988).
16. D. H. Rothman and J. Keller, *J. Stat. Phys.* **52**:1119 (1988).
17. D. H. Rothman and S. Zaleski, *J. Phys.* (Paris) **50**:2161 (1989).
18. G. R. McNamara, *Europhys. Lett.* **12**:329 (1990).

19. D. d'Humières and P. Lallemand, *Complex Systems* **1**:599–632 (1987).
20. R. Benzi, S. Succi, and M. Vergassola, *Phys. Rep.*, in press (1992).
21. A. K. Gunstensen, D. H. Rothman, S. Zaleski, and G. Zanetti, *Phys. Rev. A* **43**:4320–4327 (1991).
22. D. d'Humières and P. Lallemand, *Physica A* **140**:326–335 (1986).
23. R. Peyret and T. D. Taylor, *Computational Methods for Fluid Flow* (Springer-Verlag, 1983).
24. P. G. Saffman and Sir G. Taylor, *Proc. R. Soc. Lond. A* **245**:312 (1958).
25. G. M. Homsy, *Annu. Rev. Fluid Mech.* **19**:271 (1987).
26. R. L. Chouke, P. van Meurs, and C. van der Poel, *Trans. AIME* **216**:188 (1959).
27. D. Bensimon, L. P. Kadanoff, S. Liang, B. I. Shraiman, and C. Tang, *Rev. Mod. Phys.* **58**:978 (1986).
28. B. Shraiman and D. Bensimon, *Phys. Rev. A* **30**:2840 (1984).
29. S. K. Sarkar, *Phys. Rev. A* **31**:3468 (1985).
30. S. D. Howison, *SIAM J. Appl. Math.* **46**:20 (1986).
31. A. K. Gunstensen and D. H. Rothman, *Physica D* **47**:53–63 (1991).
32. J.-M. Aribert, Ph.D. thesis, Toulouse (1970).
33. C. T. Tan and G. M. Homsy, *Phys. Fluids* **31**(6):1330–1338 (1988).
34. P. J. Davis, *Circulant Matrices* (Wiley, New York, 1979).
35. J. A. Somers and P. C. Rem, *Physica D* **47**:39–46 (1991).